Non-Hermitian Mode Cleaning in Periodically Modulated Multimode Fibers

Mohammad Nayeem Akhter,[1] Salim B. Ivars,[1] Muriel Botey,[1] Ramon Herrero,[1] and Kestutis Staliunas[1,2,3,*]
[1]Universitat Politecnica Catalunya, Dep. de Fisica, Rambla Sant Nebridi 22, 08222, Terrassa (Barcelona), Spain
[2]Institució Catalana de Recerca i Estudis Avançats, Passeig Lluís Companys 23, 08010, Barcelona, Spain
[3]Vilnius University, Faculty of Physics, Laser Research Center, Sauletekio Ave. 10, 10223, Vilnius, Lithuania

(Received 23 November 2022; accepted 7 June 2023; published 26 July 2023)

We show that the simultaneous modulation of the propagation constant and of the gain/loss coefficient along the graded index multimode fibers results in unidirectional coupling among the modes, which leads to either the enhancement or the reduction of the excitation of higher order transverse modes, depending on the modulation parameters. In the latter case, effective mode cleaning is predicted, ideally resulting in single-mode spatially coherent output. The effect is semi-analytically predicted on a simplified Gaussian beam approximation and numerically proven by solving the wave propagation equation introducing the non-Hermitian modulated potential.

DOI: 10.1103/PhysRevLett.131.043604

Introduction.—Multimode fibers (MMFs) are currently boosting renewed attention, yet generally showing a random (speckle) output due to the different propagation constants of the fiber modes that introduce phase shifts in propagation along the fiber. Such randomization occurs even for graded index (GRIN) MMFs with parabolic index profile having equidistant propagation constants which should lead to periodic self-imaging. However, the smallest imperfections break the mode equidistance, and generally a random output is observed.

Attempts to overcome such dephasing and randomization problems have been reported, for instance, by adaptively adjusting of the phases of the modes of the input beam [1], among other means [2–4]. Recently a decrease of randomness effect, the beam self-cleaning, was proposed in Refs. [5–7]. We note, however, that the self-cleaning generally redistributes the energy among the modes preserving the integral quantities of the beam, as second order momenta in the direct and wave number space. Therefore, it does not lead to a direct reduction of the beam quality parameter, M^2.

Generally, the reduction of turbulence in optical fibers cannot be achieved by conventional means such as the modulation of refraction index, dispersion, or nonlinearity along the fiber that may indeed induce mode coupling [8,9], or to the parametric (Faraday) modulational instabilities [10–12]. However, all these effects generally broaden the angular spectra, but do not lead to a reduction of the turbulence, neither to mode cleaning.

The situation may be substantially different using a periodic *nonHermitian* modulation by simultaneously modulating the refractive index and the gain/loss coefficient along the fiber. The field of open dissipative non-Hermitian physics gained its popularity from the recently proposed parity-time (PT) symmetric systems that represent a small submanifold of the periodic non-Hermitian systems, where the phase shift between real and imaginary parts of the potential is restricted to particular values, namely, $\pi/2$ or $3\pi/2$ (for anti-PT symmetry) [13–15]. Also, the application of dynamical non-Hermitian potentials to control optical turbulence has been proposed [16–18].

Here we consider a harmonic non-Hermitian modulation along a parabolic-index MMF by the simultaneous modulation of the refractive index (propagation constant) and the gain/loss, see Fig. 1(a). Such modulations may be induced by doping the fiber core, modulating the fiber core radius and introducing some absorption, scattering, or transmission losses [19–27] (see Supplemental Material, Sec. 4 [28]).

A simple modulation of the refractive index, in the form $V(z) \sim \cos(qz) = [\exp(+iqz) + \exp(-iqz)]/2$, causes a *symmetric* mode coupling, as can be trivially inferred by the $\pm q$ exponents, which couple modes k with modes $k \pm q$ in a symmetric way, see the blue arrows in Fig. 1(c). The addition of gain/loss modulations with a spatial shift to the refractive index modulation, for instance, as $V(z) \sim \cos(qz) + i\sin(qz) = \exp(+iqz)$, *unidirectionally* couples mode k only with mode $k + q$, as represented by the green arrows. The unidirectional character of such coupling, and therefore the corresponding energy flow, may be either directed toward higher or lower index modes, depending on the shift between both modulations. Eventually, for particular phase shifts, the asymmetric coupling is expected to suppress the higher order modes, resulting in a lowest-mode coherent output. This mode-cleaning mechanism is the basic aim of the present letter.

Here, we substantize this idea: we show that the longitudinal non-Hermitian modulation of the potential

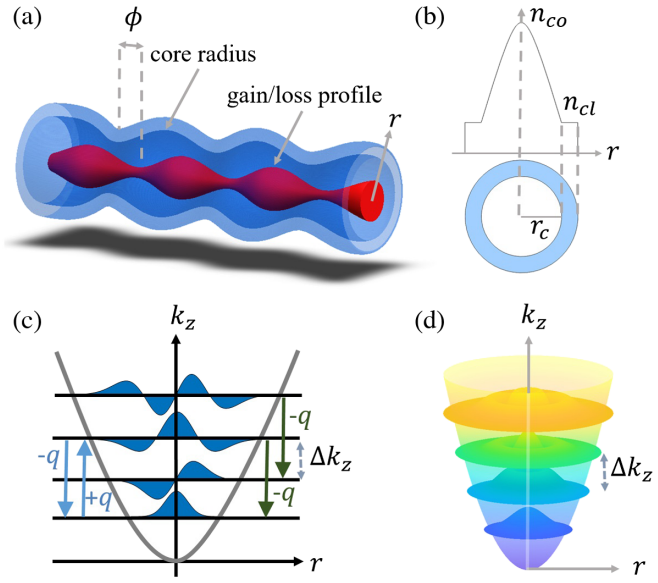

FIG. 1. (a) Periodic modulation of the core radius (Hermitian part) and gain profile (non-Hermitian part). The spatial displacement between the two modulations is indicated by a phase shift ϕ. (b) GRIN fiber cross section with a parabolic-index profile. (c) Spatial profile and cross section of the first equidistant eigenmodes. (d) 3D mode profiles.

indeed results in a tunable distribution of modes at the output. We first derive and explore a simplified model based on a Gaussian beam approximation, which predicts the effect, uncovering analytic insights, and provides estimations of the parameters. The proposal is then proven by direct numerical integration of the wave propagation equation along the fiber. On both models we analyze the modal energy distributions and, as the main result, we demonstrate a substantial condensation of radiation into the lowest order mode; resulting in a *non-Hermitian mode cleaning*.

Full model.—Light propagation in parabolic MMFs may be described by a linear Schrödinger equation as

$$\frac{\partial A}{\partial z} = i\frac{1}{2}\nabla^2 A - i\frac{\Delta}{r_c^2}r^2 A + iV(r,z)A, \tag{1}$$

where $A(x,y,z)$ is the complex field amplitude envelope in the paraxial approximation. The space coordinates are normalized to $k_0^{-1} = \lambda/2\pi$; being $k_0 = \omega_0 n_{co}/c$ the light wave number, $\nabla^2 = \partial^2/\partial x^2 + \partial^2/\partial y^2$ the Laplacian in transverse space, r_c the core radius, $\Delta = (n_{co}^2 - n_{cl}^2)/(2n_{co}^2)$ the relative index difference, and n_{co} (n_{cl}) the refractive index of the fiber core (cladding), respectively. We neglect frequency dispersion effects (as either continuous wave or sufficiently long pulses are considered), nonlinear effects and Raman scattering.

In the absence of the potential, $V(r,z) = 0$, the fields propagating in MMF exhibit a periodic self-imaging, due to equidistant mode propagation constant. The mode spacing (Δk_z) and the self-imaging period (ζ) are, respectively, given by:

$$\Delta k_z = \frac{\sqrt{2\Delta}}{r_c}, \qquad \zeta = \frac{2\pi}{\Delta k_z} = \frac{\pi r_c}{\sqrt{2\Delta}} \tag{2}$$

as follows, from Eq. (1). In the presence of a periodic potential with a periodicity close to multiples of the self-imaging period, the modes become resonantly coupled. Note that a transversally uniform potential modulation does not cause any effective coupling between transverse modes, and can be eliminated from Eq. (1) renormalizing the amplitude and phase of the propagating beam. We therefore assume a periodic modulation in z with a complex transverse profile in r: $V_{\mathrm{Re/Im}}(r,z) = V_{\mathrm{Re/Im}}(z)e^{-r^2/r_0^2}$. The fundamental concept behind this Letter is to affect the mode distribution by breaking the symmetric mode coupling which may be achieved by the introduction of a longitudinal non-Hermitian modulation in the fiber, to couple modes in a unidirectional way. We assume a complex harmonic potential in the general form:

$$V(r,z) = [m_1\cos(qz) + im_2\cos(qz+\phi)]e^{-r^2/r_0^2} \tag{3}$$

where m_1 and m_2 are the amplitudes of the refractive index and gain/loss modulations respectively, q is the modulation wavenumber, ϕ is the spatial shift between these two modulations, and r_0 is the radius of the spatial profile.

Gaussian Ansatz.—As a simple approximation of the system dynamics near the lowest transverse mode, i.e. the lowest order Laguerre-Gauss mode LG_{00}, we assume an oscillatory Gaussian ansatz of the form

$$A(r,z) = \sqrt{\rho(z)}e^{-\beta(z)r^2}, \tag{4}$$

with real-valued beam amplitude $\rho(z)$, and complex-valued beam waist $\beta(z) = \beta_r(z) + i\beta_i(z)$. The evolution of these variables as derived from Eq. (1) within the parabolic approximation reads

$$\frac{d\beta_r}{dz} = 4\beta_i\beta_r - \frac{m_2}{r_0^2}\cos(qz+\phi), \tag{5a}$$

$$\frac{d\beta_i}{dz} = 2(\beta_i^2 - \beta_r^2) + b + \frac{m_1}{r_0^2}\cos(qz), \tag{5b}$$

$$\frac{d\rho}{dz} = 4\beta_i\rho - 2m_2\cos(qz+\phi)\rho, \tag{5c}$$

where $b = \Delta/r_c^2$.

The stationary solution of Eqs. (5), in absence of modulation, $m_1 = m_2 = 0$, corresponds to the excitation of the single lowest mode of the fiber ($\beta_{r0} = \sqrt{b/2}, \beta_{i0} = 0$ and ρ_0). This regime can be achieved by a particular spatial shape of the injection into the fiber (Gaussian beam

matching the width of the lowest mode). On the contrary, a mismatched injection ($\beta_{r0} \neq \sqrt{b/2},\ \beta_{i0} \neq 0$) results in periodic solutions, with the resonance wavenumber $q = q_{\mathrm{res}} = 2\pi/\zeta = (2\sqrt{2\Delta})/r_c$, as it follows from Eq. (2), corresponding to a multimode excitation of the autonomous system. Periodic solutions with low amplitude harmonic oscillations can be found by linearizing the Eqs. (5) around its stationary solution. Such oscillations correspond to the excitation of the fundamental Gaussian mode together with higher order modes of low amplitude. The larger the modulation amplitude of the periodic solution, the stronger the excitation of higher modes. Nonharmonic periodic solutions of Eq. (5) correspond to a set of higher order modes.

The *non-autonomous* case, $m_1, m_2 \neq 0$, is more involved as it introduces the driving frequency,q, and additional stability conditions for the periodic solutions. In this case, we may rewrite Eqs. (5) in the more compact vectorial form:

$$\frac{d\vec{f}}{dz} = \widehat{NL}\,\vec{f} + \vec{p}e^{iqz}, \tag{6}$$

where $\widehat{NL}$ is the nonlinear evolution operator of the autonomous part of (5) acting on the state vector $\vec{f} = (\beta_r, \beta_i, \rho)$, and $\vec{p} = (p_1, p_2, p_3)$ is the vector of the driving amplitudes:

$$p_1 = -\frac{m_2}{r_0^2}e^{i\phi}, \qquad p_2 = \frac{m_1}{r_0^2} \quad \text{and} \quad p_3 = -2m_2 e^{i\phi}. \tag{7}$$

The solution of the driven system can be expressed as the stationary solution of the autonomous system with additional perturbations from the driving:

$$\vec{f}(z) = \overrightarrow{f_0} + \overrightarrow{\Delta f}\,e^{iqz} + \text{c.c.}, \tag{8}$$

where $\overrightarrow{f_0} = (\sqrt{b/2}, 0, \rho_0)$ is the stationary state vector, and $\overrightarrow{\Delta f}$ is the vector of driven oscillation amplitudes.

Linearization of Eq. (6) with respect to small amplitude driven oscillations leads to:

$$\hat{L} * \overrightarrow{\Delta f} = \vec{p}, \tag{9}$$

where $\hat{L}$ is the Jacobian of autonomous system of Eqs. (5). The solution of Eq. (9) is obtained by inverting the Jacobian: $\overrightarrow{\Delta f} = \widehat{L^{-1}} * \vec{p}$, and reads explicitly:

$$\overrightarrow{\Delta f} = \left(\frac{iqp_1 + q_{res}p_2}{q_{res}^2 - q^2}, \frac{iqp_2 - q_{res}p_1}{q_{res}^2 - q^2}, \frac{iq_{res}^2 p_1 \rho_0}{q\beta_{r0}(q_{res}^2 - q^2)} + \frac{q_{res}\rho_0 p_2}{\beta_{r0}(q_{res}^2 - q^2)} - \frac{ip_3\rho_0}{q}\right), \tag{10}$$

Where $q_{\mathrm{res}} = 8d\beta_{r0}$.

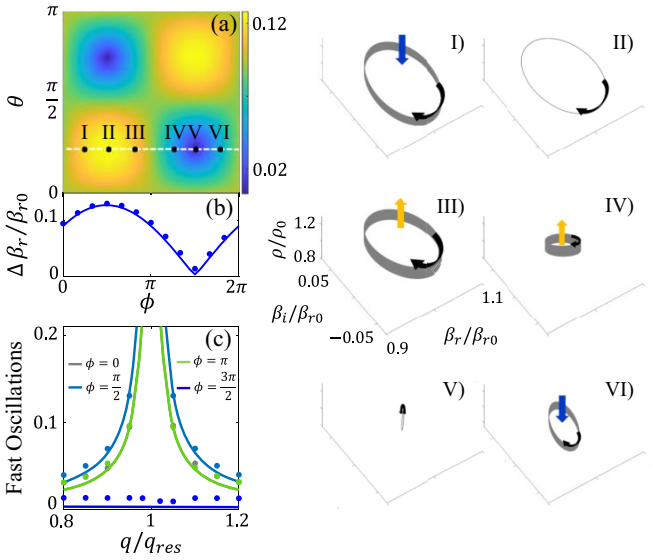

FIG. 2. (a) Map of the normalized amplitude of the beam width oscillations $\Delta\beta_r/\beta_{r0}$, in (ϕ, θ) parameter space. (b) Cross section along the white dashed line; the solid line corresponds to the simplified model, Eqs. (5), superimposed to Eq. (11). The six plots on the right-hand side show the evolution of the beam in the phase space $(\beta_r/\beta_{r0}, \beta_i/\beta_{r0}, \rho/\rho_0)$, for the different phase shifts between the two modulations, ϕ, labeled on map (a) with roman numerals, for $q = 0.95q_{res}$, $m = 8 \times 10^{-5}$. (c) Dependency of the fast oscillation on modulation frequency q for $\phi = 0, \pi/2, \pi, 3\pi/2$; the solid lines correspond to the simplified model, Eqs. (5); lines $\phi = 0$ and $\phi = \pi$ are superposed. The dots in (a),(b), and (c) correspond to the full model, Eq. (1).

The final expression of the driven oscillations of the beam waist parameter reads:

$$\Delta\beta_r = \frac{\sqrt{q^2m_2^2 + q_{res}m_1[q_{res}m_1 + 2m_2 q\sin(\phi)]}}{r_0^2(q_{res}^2 - q^2)}, \tag{11}$$

which evidences the resonant character of the solution.

Results.—We numerically integrate the system of Eqs. (5) to analyze the transient dynamics, and to check the stability of the solutions obtained by the multiscale analysis, as above described.

After normalization, Eq. (1) contains only one free parameter, Δ/r_c^2, for the unmodulated fiber, however the modulation involves five relevant parameters: m_1, m_2, ϕ, q and r_0. For convenience, we introduce m and θ as $m_1 = m\cos(\theta)$, $m_2 = m\sin(\theta)$ and numerically explore the parameter space (ϕ, θ) for a small constant value of m.

We first analyze the modulation frequency below the resonance frequency ($q < q_{\mathrm{res}}$), mapped in Fig. 2(a). The oscillations amplitude is maximum or minimum for $\phi = \pi/2$ or $\phi = 3\pi/2$. For a particular ratio between the quadratures m_1/m_2 (i.e. for particular θ), the oscillations can vanish to zero. This occurs at the shift $\phi = 3\pi/2$. Actually, Eq. (11) interprets the situation, which tells us

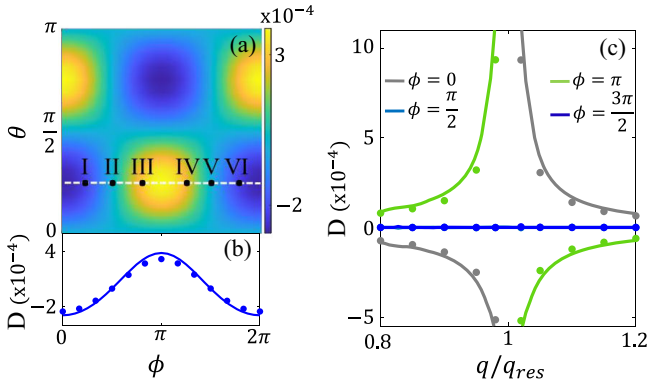

FIG. 3. (a) Map of the normalized slow drift of the intensity, $D = (\zeta d\rho/dz)/\rho_0$, in (ϕ, θ) parameter space. (b) Cross section of the map (a) along the white dashed line. (c) Dependency of the slow drift on the modulation frequency q for $\phi = 0, \pi/2, \pi, 3\pi/2$; lines $\phi = \pi/2$ and $\phi = 3\pi/2$ are superposed. In (b) and (c) the solid lines and dots correspond to the simplified model and full model.

that $\Delta\beta_r$ is minimum for $\sin(\phi) = -1$ and is maximum for $\sin(\phi) = 1$. So we can write in general,

$$\left|\frac{qm_2 - q_{res}m_1}{r_0^2(q_{res}^2 - q^2)}\right| < \Delta\beta_r < \left|\frac{qm_2 + q_{res}m_1}{r_0^2(q_{res}^2 - q^2)}\right|. \quad (12)$$

Figure 2(b) depicts the variation of the oscillation amplitude with ϕ for $\theta = \pi/4$, corresponding to the white dashed line on Fig. 2(a). The blue circular dots correspond to the numerical values, calculated from the full model described by Eq. (1), showing a good agreement between both models.

The six plots on the right-hand side of Fig. 2 depict the evolution of the system, Eqs. (5), in its phase-space, and correspond to six different non-Hermitian potentials, leading to different regimes.

We also explore the dependency of the driven oscillation amplitude, as a function of the modulation frequency of the potential. We observe that the oscillation amplitude increases as the modulation frequency approaches the resonance frequency (q_{res}) for the cases: $\phi = 0$, $\pi/2$, and π, see Fig. 2(c). The effect is maximal at $\phi = \pi/2$, is zero for $\phi = 3\pi/2$ and is same for $\phi = 0$ and π. Note the effect is symmetric as the modulation frequency passes the resonance frequency.

Interestingly, on top of the driven oscillations with the amplitude depending on the position in the phase-space of non-Hermitian driving force, the trajectory slowly drifts in the phase-space. The arrows in the six plots on the right-hand side in Fig. 2 show this behaviour. This means that the average photon number increases or decreases in propagation along the fiber. Figure 3(a) shows the dependency of the slow drift on (θ, ϕ) space. The sign of the intensity drift is controlled by the both parameters, ϕ and θ. For $m_1 = m_2$ ($\theta = \pi/4$), the drift has a maximal dependence on ϕ showing a minimum for $\phi = 0$ and a maximum for $\phi = \pi$, see Fig. 3(a). Figure 3(b) shows the variation of the slow drift with ϕ for $\theta = \pi/4$, corresponding to the white dashed line on the Fig. 3(a). The blue circular dots correspond to the full model described by Eq. (1), showing a good agreement between the simplified and full models. Cases with a negative drift (Fig. 2. I and VI) lead to a stable cycle in the (β_r, β_i) plane, while a positive drift (Fig. 2. III and IV) corresponds to unstable cycles, meaning that the beam tends to leave the Gaussian profile. Keeping the same modulation amplitude, this attainment of the limit cycle in the (β_r, β_i) plane is faster for $\phi = 0$, and requires longer propagation distances as ϕ goes from 0 to $\pi/2$. The dependency of the slow drift, as a function of the modulation frequency is provided in Fig. 3(c). Near the resonance frequency (q_{res}), we observe an asymptotic behavior for phases $\phi = 0$ and $\phi = \pi$. The intensity drift inverts its sign as the modulation frequency passes the resonance frequency and being the effect reversed for $\phi = \pi$ from $\phi = 0$. We observe no such effect for the no drift cases for $\phi = \pi/2$ and $\phi = 3\pi/2$, see Fig. 3(c).

Full numerical integration.—The previous results unveil the control of the oscillation amplitudes, demonstrating they can be reduced, leading to a monomode profile, within the demonstrated range of optimal parameters. Therefore, predicting the possibility of spatial mode-cleaning of the nosy beam. Next, we further demonstrate the effect by numerical integration of the full model of Eq. (1). A small homogeneous gain term, namely $+\gamma_0 A$, is added on the right-hand side of Eq. (1) to compensate for intensity losses, conserving the total number of photons. Speaking in experimental terms—this may be achieved by applying a slightly disbalanced gain modulation. An example of the integration, showing the evolution of a noisy beam along the MMF is displayed in Fig. 4. The highly multimodal input distribution of the beam is gradually "attracted" towards a bell-shaped transverse profile, as propagating along the fiber, see Fig. 4(a). The insets of Fig. 4(b) provide the two-dimensional transverse distribution of the beam at different propagation lengths. Figure 4(b) depicts the relative participation (OI_{pl}) of some Laguerre-Gauss modes, LG_{pl}, with low mode order N ($N = 2p + |l| + 1$), in the total field along the fiber. The participation of the lowest order mode (LG_{00}) increases tending to 1 as the beam propagates along the fiber, while the participation of higher order modes decreases. Further to characterize the beam cleaning, we calculate the evolution of the beam width in real space, angular width in Fourier space (divergence), and the beam quality factor M^2. Figures 4(c)–4(e) show a significant reduction of the beam width in both direct and wavenumber space, as the beam quality factor M^2 gradually approaches unity, acquiring an almost Gaussian profile. The mode generation either towards lower or higher order modes is confirmed by considering single mode inputs. (see Supplemental Material, Sec. 2 [28]). Finally, the robustness

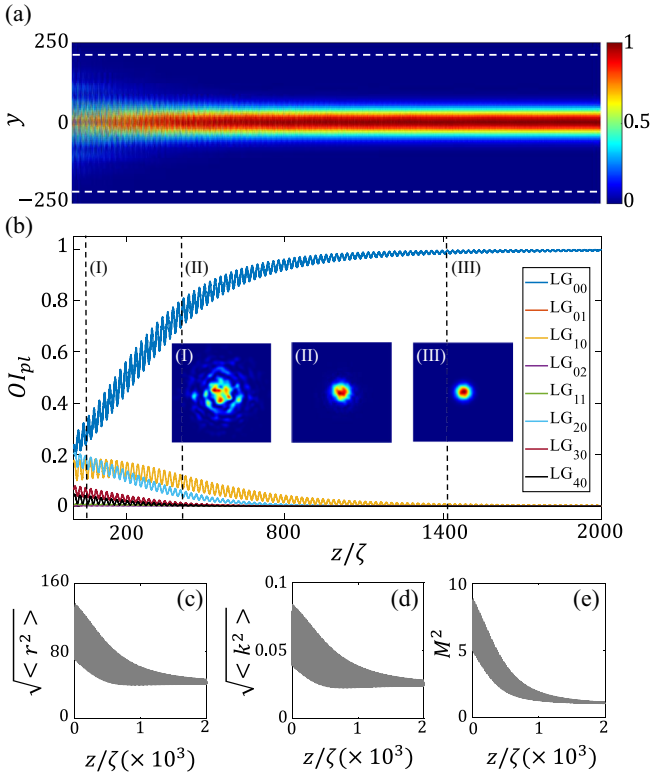

FIG. 4. (a) Evolution of the transverse noisy profile along the modulated fiber. The white dashed lines indicate the core radius. (b) Mode participation of some low order modes along the fiber. Insets: Two-dimensional transverse distributions at different propagation lengths, namely; (I) $z = 50\zeta$, (II) $z = 420\zeta$, and (III) $z = 1410\zeta$. (c) Evolution of the beam width, $\sqrt{\langle r^2 \rangle}$; (d) angular width, $\sqrt{\langle k^2 \rangle}$; and (e) beam quality factor, M^2, along the propagation distance. Fiber length is normalized to the self-imaging period ζ and $m_1 = m_2 = 2 \times 10^{-4}$, $\phi = 5.5$, $q = 0.95 q_{\mathrm{res}}$, and $\gamma_0 = 4 \times 10^{-7}$.

of this mechanism is assessed by considering deformed parabolic potentials, where the modes are not equidistant and we see that the mode-cleaning mechanism still remains effective (see Supplemental Material, Sec. 3 [28]).

Conclusions.—In conclusion, we propose and demonstrate a robust mechanism for an effective spatial mode-cleaning in GRIN MMFs. The proposal is based on the asymmetric mode coupling induced by the introduction of a non-Hermitian modulation of propagation constant and of the gain/loss coefficient along. The fiber may be modeled by a $(2 + 1)$ D Schrödinger equation with a non-Hermitian potential, where the control over the coupling among transverse modes is mainly governed by the spatial shift between the real and imaginary parts of the complex potential. The effect is first semi-analytically predicted on a simplified Gaussian beam approximation. This model provides a physical insight on the proposal, since it allows estimating the different regimes of unidirectional mode coupling either leading to spatial mode-cleaning or to higher mode excitation. The results of the integration on the full model, provides a clear numerical proof of the proposal showing a significant mode-cleaning, irrespectively of the initial intensity. The demonstrated scheme could be experimentally realized within the current nanofabrication technologies, by modulating the core radius of an amplifying fiber of length on the order of meters with distributed losses (assuming realistic parameters such as: core radius $r_c = 26$ μm, core refractive index $n_{co} = 1.47$, cladding refractive index $n_{cl} = 1.457$, the effective propagation length to observe the mode-cleaning is 1.2 m). Finally, we note that the case of coupling towards high order modes may enhance pulsing and eventually help in super-continuum generation.

This work has received funding from Horizon 2020 program project MEFISTA (Project No. 861152), from Spanish Ministry of Science, Innovation and Universities (MICINN) under Grant No. PID2019–109175 GB-C2, and from European Social Fund (Project No. 09.3.3-LMT-K712-17-0016) under grant agreement with the Research Council of Lithuania (LMTLT).

*Corresponding author.
kestutis.staliunas@icrea.cat

[1] A. Dudley, R. Vasilyeu, V. Belyi, N. Khilo, P. Ropot, and A. Forbes, Opt. Commun. **285**, 5 (2012).
[2] J. T. Murray, W. L. Austin, and R. C. Powell, Opt. Mater. **11**, 353 (1999).
[3] L. Lombard, A. Brignon, J.-P. Huignard, E. Lallier, and P. Georges, Opt. Lett. **31**, 158 (2006).
[4] W. Ha, S. Lee, Y. Jung, J. K. Kim, and K. Oh, Opt. Express **17**, 17536 (2009).
[5] K. Krupa, A. Tonello, B. M. Shalaby, M. Fabert, A. Barthélémy, G. Millot, S. Wabnitz, and V. Couderc, Nat. Photonics **11**, 237 (2017).
[6] E. Deliancourt, M. Fabert, A. Tonello, K. Krupa, A. Desfarges-Berthelemot, V. Kermene, G. Millot, A. Barthélémy, S. Wabnitz, and V. Couderc, OSA Continuum **2**, 4 (2019), https://opg.optica.org/osac/fulltext.cfm?uri=osac-2-4-1089&id=407402.
[7] L. Zhanwei, L. G. Wright, D. N. Christodoulides, and F. W. Wise, Opt. Lett. **41**, 16 (2016), https://opg.optica.org/ol/abstract.cfm?uri=ol-41-16-3675.
[8] D. Yevick and P. Danielsen, Appl. Opt. **21**, 2727 (1982).
[9] V. Garitchev, M. Golub, S. Karpeev, S. Krivoshlykov, N. Petrov, I. Sissakian, V. Soifer, W. Haubenreisser, J.-U. Jahn, and R. Willsch, Opt. Commun. **55**, 403 (1985).
[10] F. K. Abdullaev, S. Darmanyan, A. Kobyakov, and F. Lederer, Phys. Lett. A **220**, 213 (1996).
[11] M. Conforti, F. Copie, A. Mussot, A. Kudlinski, and S. Trillo, Opt. Lett. **41**, 5027 (2016).
[12] K. Staliunas, S. Longhi, and G. J. de Valcárcel, Phys. Rev. Lett. **89**, 210406 (2002).
[13] C. E. Rüter, K. G. Makris, R. El-Ganainy, D. N. Christodoulides, M. Segev, and D. Kip, Nat. Phys. **6**, 192 (2010).

[14] K. Makris, R. El-Ganainy, D. Christodoulides, and Z. H. Musslimani, Int. J. Theor. Phys. **50**, 1019 (2011).
[15] S. Longhi, Europhys. Lett. **120**, 64001 (2018).
[16] S. B. Ivars, M. Botey, R. Herrero, and K. Staliunas, Chaos Solitons Fractals **165**, 112774 (2022).
[17] W. W. Ahmed, S. Kumar, J. Medina, M. Botey, R. Herrero, and K. Staliunas, Opt. Lett. **43**, 2511 (2018).
[18] J. Medina Pardell, R. Herrero, M. Botey, and K. Staliunas, Opt. Express **29**, 23997 (2021).
[19] C. Mas Arabí, A. Kudlinski, A. Mussot, and M. Conforti, Phys. Rev. A **97**, 023803 (2018).
[20] Y. Kondo, K. Nouchi, T. Mitsuyu, M. Watanabe, P. G. Kazansky, and K. Hirao, Opt. Lett. **24**, 646 (1999).
[21] F. Hindle, E. Fertein, C. Przygodzki, F. Durr, L. Paccou, R. Bocquet, P. Niay, H. G. Limberger, and M. Douay, IEEE Photonics Technol. Lett. **16**, 1861 (2004).
[22] Y. Wang, J. Appl. Phys. **108**, 081101 (2010).
[23] J. B. Lonzaga, S. M. Avanesyan, S. C. Langford, and J. T. Dickinson, J. Appl. Phys. **94**, 4332 (2003).
[24] L. Skuja, H. Hosono, and M. Hirano, SPIE **4347**, 155 (2001).
[25] G. Cheng, L. Lin, K. Mishchik, and R. Stoian, Materials **15**, 5698 (2022).
[26] L. A. Fernandes, J. R. Grenier, P. R. Herman, J. S. Aitchison, and P. V. Marques, Opt. Express **19**, 11992 (2011).
[27] C. Hahn, E. K. Keshmarzi, S. H. Song, C. H. Oh, R. N. Tait, and P. Berini, IEEE J. Sel. Top. Quantum Electron. **22**, 48 (2016).
[28] See Supplemental Material at http://link.aps.org/supplemental/10.1103/PhysRevLett.131.043604 for additional details and discussions on unbalanced gain/loss potential, mode cascading from single mode input, robustness and fabrication.